1 *Monitoring protein structural changes and hydration in bovine meat tissue*

2 *due to salt substitutes by FTIR microspectroscopy*

3

4

5 Nebojsa Perisic[1,2*], Nils Kristian Afseth[1], Ragni Ofstad[1] and Achim Kohler[3,1]

6

7 [1]Nofima AS, Osloveien 1, N-1430 Aas, Norway

8 [2]Institute of Mathematical Sciences and Technology, Norwegian University of Life Sciences,

9 PO Box 5003, 1432 Aas, Norway

10 [3]Centre for Integrative Genetics (CIGENE), Department of Mathematical Sciences and

11 Technology (IMT), Norwegian University of Life Sciences, 1432 Aas, Norway

12

13

14

15 [*]**corresponding author:**

16 Nebojsa Perisic

17 [1]Nofima AS, Osloveien 1, N-1430 Aas, Norway

18 Phone: +47 64 97 01 00

19 Fax: +47 64 97 03 33

20 Email: nebojsa.perisic@nofima.no

21

22

Abstract

The objective of this study was to investigate the influence of NaCl and two salt substitutes, MgSO$_4$ and KCl, in different concentrations (1.5, 6.0 and 9.0 %) on meat proteins by using Fourier transform infrared (FTIR) microspectroscopy. Hydration properties and secondary structural properties of proteins were investigated by studying the amide I, amide II and water region (3500-3000 cm^{-1}) in FTIR spectra. By applying multivariate analysis (PCA and PLSR) differences between samples according to salt concentration and salt type were found and correlated to spectral bands. The most distinctive differences related to salt type were obtained by using the water region. It was found that samples salted with MgSO$_4$ exhibited hydration and subsequent denaturation of proteins at lower concentrations than those salted with NaCl. Samples salted with KCl brines showed less denaturation even at the 9.0 % concentration. The FTIR results were further supported by water binding capacity (WBC) measurements.

Keywords:

FTIR microspectroscopy, protein secondary structure, hydration, myofibrillar proteins, salt substitutes, WBC.

Introduction

In recent years, the increased consumption of dietary sodium seen in the western world has been linked to detrimental health effects (*1-3*). Thus, a need for reducing NaCl in highly consumed food products like processed industry foods (*4, 5*) has emerged. Apart from lowering down the level of added salt (NaCl) in processed foods, there are several major approaches in reducing the sodium level, while the utilization of salt substitutes is the most frequently used alternative (*4-6*). However, NaCl displays multiple functional roles in processed foods: it increases water binding capacity (WBC), inhibits microbial growth and improves taste and processability (*5*). In muscle foods, many of these properties are connected to the meat protein structure, particularly texture, tenderness and WBC (*5, 7*). When NaCl is reduced or replaced these properties inevitably change.

During the last decade a number of salt replacers has become commercially available (*8*). An appropriate salt replacer needs to have acceptable sensory properties as well as functional properties. Two candidates for successful salt replacers are KCl and $MgSO_4$, with KCl being one of the most common NaCl substitutes nowadays (*6, 9, 10*). $MgSO_4$, on the other hand, is used in some of commercially available salt mixtures replacing pure NaCl (*5, 11*).

The interaction of NaCl with the food matrix has been studied by many authors (*4, 9, 10, 12-15*), but the biophysical rational behind the mechanisms of the interaction between NaCl and the protein matrix in muscle foods is still only partially understood. In recent years, Fourier transform infrared (FTIR) microspectroscopy has been used for monitoring conformational changes of myofibre proteins. By utilization of FTIR microspectroscopy, *in situ* spectra of single myofibre cells can be obtained. Böcker et al. showed by employing FTIR microspectroscopy that changes in tertiary structure of the myofibers during swelling and shrinkage may be directly related to changes in the secondary structure of myosin molecules (*16*). FTIR microspectroscopy has also been employed to study conformational changes in

66 proteins as a function of salt concentration (*16*). Furthermore, in combined FTIR and low

67 field NMR studies conformational changes in proteins due to different salt concentrations

68 have been related to water binding properties (*17, 18*). Since it is very likely that salt replacers

69 change the biophysical situation on a molecular level, similar studies involving different salt

70 replacers are urgently needed. Moreover, it is known that FTIR spectroscopy can also provide

71 information about water molecules interacting with protein molecules and salt ions (*19-21*).

72 This potential has yet to be utilized for studying the interaction between salt substitutes and

73 meat matrices.

74 The main objective of this study was to investigate and assess the differences in the effects of

75 NaCl, KCl and $MgSO_4$ on the protein structure and hydration properties in bovine meat using

76 FTIR microspectroscopy. In order to do this we used FTIR spectra to:

77 (I) determine changes in protein secondary structure and water interactions through analyzing

78 the amide I (1600-1700 cm^{-1}) and the amide II regions (1500-1600 cm^{-1}),

79 (II) assess and estimate the interaction of protein molecules with water through analyzing the

80 region between 3000 and 3500 cm^{-1}, denoted as the "water region" that also includes amide A

81 and amide B bands (*22*), as well as information about the OH stretching vibration of water

82 molecules, and

83 (III) correlate these different sample characteristics by using multivariate analytical methods

84 based on latent variables, such as principal component analysis (PCA) and partial least

85 squares regression (PLSR).

86 Band assignment of respective underlying bands in all selected regions has also been

87 attempted both in accordance to literature and to multivariate data analysis. In addition,

88 measurement of water binding capacity (WBC) of brined meat was performed to validate the

89 results obtained by FTIR microspectroscopy.

90

Materials & Methods

Sample preparation: Samples of beef muscle (*longissimus dorsi*) were obtained from four different animals (breed: Norwegian Red) after 48 hours post rigor (obtained from a commercial slaughter). From each animal, two muscle blocks of approximately $4 \times 4 \times 1$ cm were excised and placed in each of 9 different salt brines. The salt brines were comprised of pure NaCl, KCl and $MgSO_4$ (Merck, Germany) solutions, made in 1.5 %, 6.0 % and 9.0 % total salt weight percentage concentration. To avoid dilution of the salt brines, the mass ratio of meat to brine was set to approximately 1:8. The samples were kept in brines at 4 ℃ for 48 hours with 0.05 % NaN_3 added in order to prevent any possible deterioration caused by microbial growth.

Water binding capacity: Commercially available fresh samples of beef muscle (*longissimus dorsi)* were obtained and consecutively brined in the same way as aforementioned. From each of the 4 commercial packages two slices of 3 x 3 x 1 cm were excised and placed in each brine, resulting in a total of 8 replicates in each of the 9 salt brines. Afterwards, the expressed juice was measured by the filter paper press method (*23*): meat samples were placed between 5 layers of filter paper (Whatman 1, 70 mm diameter) and consecutively pressed by aluminum plates using a TA.HDi Texture Analyser (Stable Micro Systems Ltd, England), with a velocity of 0.8 mm/s until a 50 % reduction of the sample thickness. After the 50 % sample thickness reduction was reached, the plates were immediately pulled back. The percentage of expressed juice was calculated as the mass of expressed juice divided by the initial sample mass (i.e. the sample mass before applying pressure).

FTIR microspectroscopy: For FTIR microspectroscopic measurements, two muscle blocks of approximately 1.0 x 0.6 x 0.3 cm were excised from each of the muscle samples, consecutively embedded in O.C.T. compound (Tissue-Trek, Electron Microscopy Sciences, Hatfiles, USA), and snap-frozen in liquid N_2. Afterwards, all of the samples were transferred

116 to a -80 ºC freezer where they were stored until cryo-sectioning, which was performed

117 transversely to the fiber direction on a Leica CM 3050 S cryostat (Leica Microsystems

118 Wetzlar GmbH, Wetzlar Germany). The sections were cut in 10 μm thickness, thaw-mounted

119 on infrared transparent ZnSe slides and subsequently stored in a desiccator before acquisition

120 of the FTIR spectra.

121 Acquisition of FTIR spectra was performed on an IRScopeII FTIR microscope coupled to an

122 Equinox 55 FTIR spectrometer (Bruker Optik GmbH, Ettlingen, Germany), equipped with a

123 liquid nitrogen-cooled mercury cadmium telluride (MCT) detector. Spectra were collected

124 from single myofibers in transmission mode in the range from 4000 to 1000 cm^{-1}, with

125 spectral resolution of 4 cm^{-1} using a 15X objective lens.

126 For each spectrum 64 interferograms were collected and averaged. Both spectrometer and

127 microscope were sealed by a specially designed box and were continuously purged with dry

128 air in order to reduce the spectral contribution of water vapor and CO_2. Additional

129 compensation for water vapor/CO_2 variation was accomplished by taking background spectra

130 of the ZnSe substrate. From each of the snap-frozen meat blocks (1.0 x 0.6 x 0.3 cm) 2 cryo-

131 sections were excised, and from each of the cryo-sections 15 spectra were obtained on

132 different single myofibers. This resulted in acquisition of 30 spectra per experimental

133 treatment and animal. The final data set consists of 1080 spectra (30 spectra times 4 animals

134 times 9 brines).

135 **Data analysis:** Spectra were subjected to a quality test developed by Bruker (Bruker Optik

136 GmbH, Ettlingen, Germany) which involves testing spectra for signal-to-noise ratio, signal

137 intensity and water vapor amount within the predefined limits for each of the criteria. Spectra

138 not passing the predefined limits were removed.

139 Second derivatives of the spectra were calculated using the Savitzky-Golay algorithm (*24*) in

140 order to resolve the overlapping bands of individual vibrations in three different regions:

141   water region (3500-3000 cm^{-1}), amide I region (1700-1600 cm^{-1}) and amide II region (1600-

142   1500 cm^{-1}). Since the bands in the water region are generally much broader and the water

143   region is also subjected to a higher level of water vapor, a bigger window for calculating

144   second derivative by the Savitzky-Golay algorithm was used in this region: a window of 37

145   smoothing points was used for the water region, while in the amide I and amide II regions, we

146   applied a window size of 11 smoothing points. Since spectral reading was approximately one

147   absorbance value per cm^{-1}, the window size for calculating second derivative in water region

148   corresponds to approximately 36 cm^{-1}, while in amide I and II regions it corresponds to

149   approximately 11 cm^{-1}.

150   The spectra were thereafter averaged by taking the mean of all replicate spectra of the same

151   muscle block, resulting in 4 spectra per brine and animal (2 muscle blocks times 2 cryo

152   sections). Afterwards, the spectra were pre-processed using extended multiplicative signal

153   correction (EMSC) (*25, 26*) in region 1800-1000 cm^{-1} for amide I and II region and 4000-

154   1000 cm^{-1} for water region bands. This provides the ability to separate and characterize the

155   unwanted physical effects (e.g. differences in sample thickness and light scattering) and

156   desired chemical information (e.g. protein secondary structure) that are contained in the

157   spectra *(25)*.

158   After pre-processing, the data were analyzed by principal component analysis (PCA) and

159   partial least square regression (PLSR) (*27*). PCA was used to study the unsupervised variation

160   pattern in the data (*28*) and partial least squares regression (PLSR) was performed in order to

161   relate different spectral regions. In PLSR models, the water region was used as *X* matrix,

162   while as *Y* matrix amide I and amide II regions were used separately. Correlations between

163   FTIR variables, design variables and latent variables were studied by correlation loading

164   plots, in which the correlations between variables and PLS/PCA score vectors are plotted. In

165   correlation loading plots both variables that were part of the PCA/PLSR modeling and

166   variables that were kept outside the modeling step were plotted. Design variables were never

167   used to build PCA or PLSR models. When design variables were plotted in correlation

168   loading plots, they were defined as indicator variables, i.e. one column for each design

169   variable in which 1's and 0's indicate if the sample belongs to the respective design condition

170   or not, respectively. All PCA and PLSR results are consecutively validated by cross-

171   validation (*29, 30*), where samples referring to the same animal are taken out in each cross-

172   validation loop. All variables are divided by their standard deviation before analysis by PCA

173   and PLSR.

174   For calculating PCA and PLSR models, whole FTIR regions including all variables were

175   used. For the sake of clarity, the correlation loading plots were presented by using only

176   positions of the minima in second derivative spectra, which correspond to positions of band

177   maxima in non-derivative spectra. Certain FTIR bands exhibit shift in minima position. In the

178   plots this is manifested as continual assembly of variables close to each other and is

179   particularly visible in water region variables.

180   Pre-processing and data analysis were performed using in-house developed routines written in

181   MATLAB (version 7.10 The MathWorks, Natick, MA) and The Unscrambler (version 10.1

182   CAMO Process AS, Norway).

183

184   ## Results

185   ### Band assignment

186   Examples of FTIR spectra obtained from single myofibers from tissue sections are shown in

187   Fig. 1. Specific regions of the FTIR spectra that were used for the analysis are marked with

188   grey shades in Fig. 1a and include the water region (3500-3000 cm^{-1}), the amide I region

189   (1700-1600 cm^{-1}), and the amide II region (1600-1500 cm^{-1}). Second derivative spectra of

190   these three regions are shown in Fig. 1b, c and d, respectively. Correspondingly, a summary

191 of tentative assignments of the bands, which is in accordance with our previous work and

192 literature (*18, 31*) is given in Table 1. As it has been shown, each of these regions provides a

193 specific type of information on protein structure and protein hydration, which is available

194 through analyzing the properties of vibrations that the specific region is comprised of. More

195 specifically, the amide I region (1700-1600 cm^{-1}) presented in Fig. 1c provides detailed

196 information about the protein backbone, mainly through dominating contributions of the C=O

197 stretching vibration (*20, 32*). Due to its high sensitivity to protein secondary structure, the

198 amide I band is often used to study protein folding, unfolding and aggregation. The amide II

199 region (1600-1500 cm^{-1}) that is presented in Fig. 1d consists mainly of N-H in-plane bending

200 and C-N stretching vibrations (*32*). The assignment of bands in the amide II region is not as

201 clear as in the amide I region, which is why the latter region is often preferred in protein

202 structure analysis by FTIR spectroscopy (*22*). Finally, the water region (3500-3000 cm^{-1})

203 presented in Fig. 1b consists mostly of N-H stretching vibrations and O-H stretching bands,

204 including the amide A and B bands (*19, 22*).

205

206 **PCA results – protein-water interactions**

207 In order to study differences in protein structures and hydration properties as a function of salt

208 concentration and salt type, principal component analysis was performed on second derivative

209 spectra of the amide I region and the water region, separately. Score plots for the first and

210 second principal components (PCs) for both regions are presented in Fig. 2. Score plots of the

211 amide I region variables are presented in the first row of Fig. 2 (Fig. 2a and 2b), while score

212 plots of the water region variables are presented in the second row (Fig. 2c and 2d). Labeling

213 of samples was done with respect to the experimental design: salt concentration label (first

214 column of Fig. 2a and 2c) and salt type label (second column of Fig. 2b and 2d).

Amide I: As it can be seen in Fig. 2a, the effect of salt concentration spans most of the variation in the amide I variables, causing samples that are treated with different salt concentrations to cluster together. The calibrated explained variance for PC1 is 54.5 %, while the validated explained variance is 53.6 %. The first PC accounts for most of this concentration effect, since the major part of the 9 % samples is clearly separated from the rest of the samples along the PC1. Furthermore, on the same figure it is visible that the 1.5 % samples are clearly separated from the rest of samples along PC2. The calibrated explained variance for PC2 is 16.9 %, while the validated explained variance is 16.5 %. We can also see that within the different concentration clusters (visible in Fig. 2a), there is a minor degree of separation with respect to salt type (Fig. 2b). The effect of different animals was also investigated, but the score plots did not show any visible clustering of samples due to animal type (results not shown). This leads to the conclusion that the effect of different animals is much smaller than effects of salt type and salt concentration and that this effect as such does not significantly affect the differentiation between samples.

Water region: Unlike in the amide I region, clustering of samples is visible for both salt type and salt concentration in the water region as presented in Fig. 2c and 2d. Within the clusters due to salt type, sub-clusters due to concentration are also visible. The calibrated explained variance for PC1 is 60.5 %, while the validated explained variance is 60.3 %. In the first PC a clear distinction between KCl and NaCl brines is visible, while the difference between $MgSO_4$ (bottom) and NaCl and KCl brines (top) is visible in PC2. The calibrated explained variance for PC2 is 18.1 %, while the validated explained variance is 17.9 %. Similarly to the amide I region clusters due to the different animals are not visible in score plots of water region variables (results not shown).

In order to assess specific spectral features that are causing the distinction of the samples presented in the PCA score plots, the corresponding correlation loading plots are displayed.

240   The correlation loading plots of these PCA models are presented in Fig. 3. More precisely, the

241   Fig. 3a depicts the correlation loading plot of PC1 and PC2 of the amide I region, including

242   design variables. Equivalently, Fig. 3b depicts the correlation loading plot of PC1 and PC2 of

243   the water region variables, including design variables. Since the score plots showed

244   tendencies of interactions between certain salt types and concentrations such as between

245     $MgSO_4$ salt type and 6 % concentration, all possible interactions between design variables are

246   included and presented in the plots. Interaction variables are simply calculated as products of

247   the design variables.

248   **Amide I** (see **Fig. 3a**)**:** The main variation in the *positive* direction of PC1 is due to variables

249   around bands assigned to aggregated β-structures at 1630 and 1693 cm^{-1} (*32-35*) and anti-

250   parallel β-structures at 1683 cm^{-1} (*22, 33*). In some specific cases these bands are also

251   associated with protein hydration differences (*19*). The main variation in the *negative*

252   direction of PC1 is due to variables around a band at 1655 cm^{-1} related to native α-helical

253   structures and water vibration (*20, 32, 33, 36-38*) and variables around a yet non-assigned

254   band at 1614 cm^{-1}. Thus, the design variables 9 % salt concentration, 9 % NaCl and 9 %

255     $MgSO_4$ brines are strongly *positively* correlated to bands attributed to aggregated β-structures.

256   The main variation in PC2 may be explained by a shift of the band at 1655 cm^{-1} from higher

257   to lower wavenumbers, while the lower wavenumbers are shifted towards the *positive*

258   direction of PC2. In addition to this, a band assigned to non-hydrogenated C=O groups at

259   around 1668 cm^{-1} (*32, 35*) and a band tentatively assigned to turns (*22*) at 1674 cm^{-1} are

260   *negatively* correlated to PC2. The design factors related to 1.5 % salt concentration brines and

261   1.5 % of NaCl brines are both *positively* correlated to PC2, although this correlation is not

262   very strong.

263   **Water region** (see **Fig. 3b**)**:** The first PC of the PCA model of the water region variables is

264   explained by a shift from wavenumbers 3283 cm^{-1} to 3290 cm^{-1}. The corresponding band

265 around 3290 cm^{-1} is assigned to the amide A band (between 3270 and 3310 cm^{-1}), which is

266 exclusively located on the NH group and for that reason is not sensitive to the conformation

267 of the polypeptide backbone in proteins (*22*). However, the frequency of this band depends on

268 the strength of the hydrogen bond (*22*). A band around 3063 cm^{-1} and a band around 3361cm^{-1}

269 are explaining a major part of the variation along PC2. The band around 3063 cm^{-1} together

270 with the design factors related to NaCl salt brines is *positively* correlated to the PC2. This

271 band is assigned to amide B, the second part of the Fermi resonance doublet (with amide A

272 being the first part) absorbing weakly between 3100 and 3030 cm^{-1} (*22*). In small peptide

273 molecules this band is attributed to the overtone of the amide II vibration and in β-sheet

274 structures it is associated with the amide II combination mode (*22*). Alternatively, this same

275 band is assigned to NH stretching vibrations of intra-molecularly hydrogen bonded NH

276 groups (*22, 39*). The band at 3361cm^{-1} which is *negatively* correlated with PC2 is assigned to

277 both the N-H stretching band and the amide II overtone (*19, 22, 39*). A band around 3420 cm^{-1}

278 (*19, 22*) which is assigned to non-hydrogenated NH groups and a band around 3120 which is

279 not assigned (and also appears as a shoulder to the 3190 cm^{-1} band) are also *negatively*

280 correlated to PC2. Design variables related to KCl brines are weakly *negatively* correlated to

281 PC1. The design variables referring to MgSO$_4$ brines are *negatively* correlated to PC2, and

282 therefore strongly *positively* correlated to non-hydrogenated NH groups.

283 In addition to this, higher principal components were also taken into consideration (data not

284 shown). The variation explained by these components enabled only the distinction between

285 low (1.5 %) and higher (6 and 9 %) salt concentrations (only in PC 3 and 4), and no

286 significant variance due to different salt types were found.

287

288 **PLSR results**

289 In order to relate information about protein conformations, hydrogen bindings and water, a

290 PLSR was performed. For this purpose water region variables were used as X, and the amide I

291 and II regions were defined as Y. The corresponding correlation loading plots are shown in

292 Fig. 4a and Fig. 4b, respectively. Design variables including interactions between salt

293 concentrations and salt types were pacified in the calculation of the PLSR models, such that

294 they were not affecting the model. The X variables are plotted in black color, Y in blue and

295 design variables in green. It can be seen that all applied salt types explain variations with

296 respect to secondary structure of proteins combined with protein hydration (both amide I and

297 amide II defined as Y variables) and their hydration properties (X variables). The same is

298 apparent for the applied concentrations.

299 **Amide I (Y) and water region (X)** (Fig. 4a): The first component is explaining 30.4%/27.6%

300 of the variance in the X and Y blocks, respectively. After validating this model by cross-

301 validation, the explained variance for PC1 is 29.3%/26.6% for X and Y respectively. Further,

302 bands at 1631 cm^{-1} (aggregated β-structures) ([32-35]), 1682 cm^{-1} (antiparallel β-sheet

303 structures) ([20, 32, 33, 37]), 1638 cm^{-1} (assigned to aggregated β-structures or water

304 deformation mode) ([36, 38]) and bands at around 3400 cm^{-1} (assigned to hydrogenated N-H

305 groups or OH stretching vibration) ([19, 22, 39]) are *positively* correlated to PC1 and therefore

306 also *positively* correlated to design variables 9 % MgSO$_4$, MgSO$_4$ and 9 % concentration. The

307 main variation in the *negative* direction of PC1 is due to bands at 1655 cm^{-1} (α-helical

308 structures), 1616 cm^{-1} (possibly tyrosine)([33, 40]), 1674 cm^{-1} (turns), 3190 cm^{-1} and 3035 cm^{-1}

309 (not assigned). The band at around 1655 cm^{-1} is also known to be related to water vibrations

310 ([36, 38]). However, in our correlation loading plots this band is always negatively correlated to

311 vibrational bands of hydrogenated NH groups at above 3400 cm^{-1} and at 1638 cm^{-1} band

312 attributed to water bending vibration (Fig. 3a and 4), and therefore we are mainly attributing it

313 to protein α-helical structures and corresponding hydration changes. The design variables 6 %

314   salts, 6 % KCl, KCl brines and 6 NaCl brines are also *negatively* correlated to PC1. The

315   second component is explaining 25.1%/12.1% of the variance in the *X* and *Y* blocks,

316   respectively (after cross-validation 24.9%/11.6%). In the *positive* direction of PC2 the main

317   variation is due to N-H stretching vibration at 3063 cm^{-1} (somewhat ambiguously assigned to

318   amide II overtone, amide B and intra-molecularly hydrogen bonded NH groups) (*22, 39*) and

319   1674 cm^{-1}. The design variable 6 % NaCl is close to the band at 1674 cm^{-1} in the correlation

320   loading plot. Design variables 9 % NaCl and 6 % NaCl and NaCl are *positively* correlated to

321   PC2 and thus to amide II overtones. Variables around 3125 cm^{-1} and a band at 1618 cm^{-1} are

322   contributing the most to the main variation in the *negative* direction of PC2,. The variables

323   around 3125 cm^{-1} refer to a not assigned and very weak shoulder in the spectra, while the

324   band around 1618 cm^{-1} has previously been assigned to tyrosine (*40, 41*) or protein-water

325   interaction in casein micelles investigation (*36*). Both bands are strongly *positively* correlated

326   to the design variables 1.5% MgSO$_4$, 6 % MgSO$_4$ and MgSO$_4$ as well as to design variables

327   1.5 % KCl and 1.5 %.

328   **Amide II (*Y*) and water region (*X*)** (Fig. 4b): The first component is explaining

329   33.7%/25.1% of the variation in the *X* and *Y* blocks, respectively (after cross-validation

330   32.8%/24.3%). The variation in the *positive* direction of PC1 is mostly due to bands assigned

331   to non-hydrogenated N-H groups at above 3400 cm^{-1}. These bands are strongly correlated to

332   MgSO$_4$ brines, since the design variables 6 % MgSO$_4$, 9 % MgSO$_4$ and MgSO$_4$ are all

333   *positively* correlated to PC1, while 9 % MgSO$_4$ and MgSO$_4$ are somewhat stronger correlated.

334   The main variation in the *negative* PC1 direction is mainly due to a band at 1584 cm^{-1}

335   assigned to α-helical structures (*33*), and bands at 3190 cm^{-1}, 3035 cm^{-1} (both not assigned)

336   and a band around 1575 cm^{-1} which is assigned to amide II without further specification (*33*).

337   These bands are *positively* correlated to the design variables KCl brines, 6% KCl and 6 %

338   concentration. PC2 accounts for 19.1%/11.6% of the variance in the *X* and *Y* blocks,

339 respectively (after cross-validation 17.34%/9.3%). The main variation in the *positive* direction

340 of PC2 is due to the band at 1516 cm^{-1} which is assigned to tyrosine (*33, 40*) and a band at

341 3063 cm^{-1} assigned to the N-H stretching band of the amide II overtone (*22, 39*). The design

342 variables 9 % brines and 6 % NaCl and 9 % NaCl are *positively* correlated to these bands. The

343 main variation in the *negative* PC2 direction is due to variables close to but below the band at

344 1572 cm^{-1} (not assigned) with a very weak contribution of the band at 1567 cm^{-1} which is

345 ambiguously assigned to either amino acid side-chain residues (*22, 42*) or aggregated β-

346 structures (*33*). Design variables that are closely related to these bands are 1.5 % brines, 1.5 %

347 Na, 1.5 % KCl and 1.5 % MgSO$_4$ brines.

348 PLSR models were also established by splitting the data in subsets where each subset

349 corresponded to one concentration (1.5 %, 6% and 9 % brines). For each concentration

350 separately, the variation introduced by the different salt types was studied. In Fig. 5, the

351 correlation loading plot for the PLSR model of the 6 % concentration is presented. The model

352 was calculated using water region variables as *X* and amide I variables as *Y* variables, while

353 amide II and design variables were pacified and plotted together with the other variables in

354 the correlation loading plot. The first component is explaining 48.2%/27.2% of the variation

355 in the *X* and *Y* blocks, respectively (after cross-validation 45.4%/23.3%). The main variation

356 in the *positive* direction of PC1 is caused by variables around the bands at 1674 cm^{-1} (turns),

357 3035 cm^{-1} (not assigned) and 3190 cm^{-1} (not assigned). All these bands are strongly *positively*

358 correlated to variables around the amide II bands at 1594 cm^{-1} and 1584 cm^{-1}. The main

359 variation in the *negative* direction of PC1 is caused by the variables around the bands at above

360 3400 cm^{-1} (hydrogenated N-H groups), at 3290 cm^{-1} (N-H stretching band, amide A or

361 hydrogen bonded NH groups) (*21, 22, 39, 42*), at 1631 cm^{-1} (aggregated β-structures) and

362 1682 cm^{-1} (antiparallel β-structures). All these bands are strongly *positively* correlated to

363 MgSO$_4$ salts. The second component is explaining 12.8%/19.1% of the variation in the *X* and

364   *Y* blocks, respectively (after cross-validation 5.2%/3.6%). Variables around the amide I bands

365   at 1638 cm^{-1}, 1690 cm^{-1} and 1682 cm^{-1} are *positively* correlated to PC2 and thus *positively*

366   related to bands around the 1537 cm^{-1} band which have been assigned to aggregated β-

367   structures. Variables around the bands at 1611 cm^{-1} and 1618 cm^{-1} are *negatively* correlated to

368   PC2.

369   **<u>Water Binding Capacity (WBC)</u>**

370   In order to elucidate the relationship between water binding capacity and the observed

371   differences in protein hydration and denaturation characteristics between the different salts, an

372   additional experiment was performed. The results from water binding capacity measurements

373   are presented in Fig. 6, where the percentage of expressed juice is plotted for each brine. As it

374   can be seen, the overall trend is that with increasing concentration of salt, the amount of

375   expressed juice is decreasing (from 10.5 % to 5.1 % for NaCl brines, from 8.4 % to 4.5 % for

376     $MgSO_4$, and from 11.0 % to 8.4 % for KCl brines), which directly corresponds to increased

377   WBC. The highest WBC (lowest amount of expressed juice) in the 1.5 % concentration range

378   is found in samples treated with $MgSO_4$ (8.4 %), while the lowest WBC is found for KCl

379   (11.0%), which was also close to samples treated with NaCl (10.5 %). Overall, samples

380   treated with $MgSO_4$ exhibit higher similarity to samples treated with NaCl than to samples

381   treated with KCl. Finally, samples treated with $MgSO_4$ brines exhibit the highest WBC in all

382   of the applied concentrations. The results obtained by WBC measurements show a high

383   correspondence to the results obtained by FTIR microscopy. This again is showing that the

384   changes in the secondary structure of the myofibrillar proteins can be connected to

385   macroscopic properties of meat, such as WBC.

386

387   ## Discussion

388   **<u>Myofibrillar proteins: secondary structure, hydration and denaturation</u>**

389   Salting of meat is associated with changes in the water binding capacity of the meat proteins

390   and it is also linked to protein destabilization and denaturation when salt concentration

391   increases (*16, 33*). Destabilization and denaturation of proteins in meat tissues as well as their

392   hydration can be monitored in the amide I region (1700-1600 cm^{-1}) and the water region

393   (3500-3000 cm^{-1}) of FTIR spectra. The amide I region (Fig. 1b) provides detailed information

394   about protein backbone, mainly through dominating contributions of the C=O stretching

395   vibration (*20, 32*). The analysis of the PCA score plots made on the amide I region (Fig. 2a-c)

396   unveils that the main variation pattern in the amide I region is caused by differences in salt

397   concentration. This difference in salt concentration also seems to be the main factor for

398   protein secondary structural changes in the meat proteins in the present experiment. When

399   examining the corresponding correlation loading plot in Fig. 3a, we can see that high salt

400   concentrations are related to the band at ~1631 cm^{-1} together with a weaker band at around

401   1693 cm^{-1}, which have been assigned to aggregated β-structures in meat tissue samples (*32,*

402   *34, 35*). The increase in intensity of this band corresponds to increase in amounts of

403   aggregated β-structures. This is also often followed by a decrease in intensity of the band at

404   ~1655 cm^{-1}, a pronounced intensive band with a weak shoulder occurring at lower

405   wavenumbers, that can be assigned to C=O stretching vibrations originating from α-helical

406   structures in the myofibrillar proteins (*20, 32, 33, 37*) and to water vibrations (*36, 38*).

407   Conversely, the α-helical band around 1655 cm^{-1} is located at the opposite side of the

408   aggregated structures and hydrogenated NH groups in the correlation loading plot in Fig. 3a,

409   which shows that the increase of aggregated structures with high salt concentrations is related

410   to a decrease of α-helical structures in the studied myofibrillar proteins. This finding is in

411   agreement with literature (*16, 31*), where a rise in NaCl concentration in brine salting of pork

412   meat was found to be inducing an increase in non-hydrogenated C=O groups and aggregated

413   β-structures at the expense of native α-helical structures (*16, 33, 43*). On the other hand, the

414   amide I band occurring at around 1618 cm^{-1} is tentatively assigned to aggregated β-structures

415   (*17, 33, 43*). This finding is not in accordance to our results, where this band is often

416   correlated to the lowest salt concentration (most of these results not shown here) and to bands

417   that are assigned to hydrogenated NH groups. In our data the band at 1618 cm^{-1} also exhibits a

418   *negative* correlation tendency towards aggregated β-structures (that are mostly detectable

419   through the band at 1631 cm^{-1}). However, in our results this band does not show any clear

420   pattern in correlation tendencies and therefore remains not assigned.

421   Along with this, the water region (3500-3000 cm^{-1}) presented in Fig. 1b consists mostly of N-

422   H stretching vibrations and O-H stretching bands (*19, 22*). The analysis of the score plots of

423   the PCA of the water region in Fig. 2c and 2d shows that the main variation pattern in the

424   water region is caused by different salt types. Within each salt type cluster there are visible

425   concentration differences, but they are obviously less pronounced than the differences due to

426   salt types, meaning that the differences between types of salts applied are causing larger

427   alterations in protein hydration than differences in applied salt concentrations. While the first

428   component to some extent separates the NaCl samples from the KCl samples, the second

429   component shows a clear separation of $MgSO_4$ from the NaCl and the KCl treated samples. In

430   the corresponding correlation loading plot in Fig. 3b it can be seen that the region 3500-3450

431   cm^{-1} is *positively* correlated to $MgSO_4$ salt type in high concentrations. In this region the

432   intermolecular $\nu_{O\text{-}H}$ stretching band is located. It is most pronounced in liquid water spectra

433   with maximum around 3430-3420 cm^{-1} and is also present in dry hydrated bio-molecules with

434   a shift towards lower wavenumber due to smaller amount of H-bonds (*19*). This is in

435   correspondence with the WBC results (Fig. 6) that show highest WBC for samples treated

436   with 9 % of $MgSO_4$ (4.5 % of expressed juice compared to 5.1 % of NaCl and 8.4 % of KCl).

437   As can be seen in Fig. 3b, the $\nu_{O\text{-}H}$ stretching band exhibits a shift stretching from 3411 cm^{-1}

438   close to the design variable 9 % NaCl to the design variable 9 % $MgSO_4$ while passing close

439   by the design variable 9 % concentration. This shows that hydration is increased for higher

440   salt concentrations and that there is some interaction effects between the salt type factors of

441   NaCl and MgSO$_4$ and the concentration factor of 9 %, corresponding also to the similarities

442   found in the values of WBC for these two salt types.

443   In order to address the protein structural information directly, the information about water

444   binding in the amide I region was related to the water region by PLSR. The corresponding

445   correlation loading plot is shown in Fig. 4a. In this figure the same tendencies as in Fig. 3a

446   and 3b can be observed, with a difference that in Fig. 4a the relationship between the water

447   binding and the protein region is much clearer. In addition to this, an increased salt

448   concentration causes an increment of intensity in the intermolecular ν_{O-H} stretching occurring

449   around 3430-3420 cm^{-1}. This is the case for MgSO$_4$ and NaCl, but not for KCl brines. This is

450   also apparent in WBC measurements, where KCl treated samples exhibit the lowest WBC,

451   while NaCl and MgSO$_4$ brines cause similar effects to the WBC of the meat samples.

452   Moreover, there is a clear interaction effect visible between the MgSO$_4$ and NaCl salt types

453   and the 9 % salt concentration, while the interaction variable 9 % KCl is not related to high

454   hydration levels. It can also be seen that the increase of hydration is closely related to the

455   aggregated β-structures. This again can be interpreted in the way that with increasing

456   hydration, proteins unfold and increase the water binding capacity by exposing larger parts of

457   the protein molecules to water (*44, 45*). The exposure of the hydrophobic part leads then

458   finally to a destabilization and partial denaturation of the myofibrillar proteins at the highest

459   salt concentrations (in addition to thermal effects and effects of pH)(*46*), which is expressed

460   by the *positive* correlation of the band ~1631 cm^{-1} with the interaction variables 9 % MgSO$_4$

461   and 9 % NaCl and the concentration variable 9 % in Fig. 3b and Fig. 4a.

462   In Fig. 3b and 4 it can also be seen that there is a remarkably strong correlation between the

463   hydration bands (around 3430-3420 cm^{-1}), the water or aggregated β-structure band at 1638

464   cm^{-1} and the interaction factor 9 % MgSO$_4$ and the salt type MgSO$_4$. At the same time there is

465   also a clear correlation between this hydration band and the band of aggregated β-structures.

466   A correspondingly strong correlation between aggregated β-structures around 1631 cm^{-1} and

467   the interaction variable 9 % MgSO$_4$ can be seen. It seems that MgSO$_4$ has a stronger effect on

468   hydration and denaturation of the proteins than NaCl. Since the effect of salts alone in the

469   applied concentrations is not sufficient for complete unfolding and denaturation of proteins, it

470   is likely that the investigated proteins are partially unfolded and therefore their hydration is

471   notably altered in a direction of increased hydration. We may also hypothesize that MgSO$_4$

472   causes higher partial denaturation and increased subsequent hydration at lower concentrations

473   than NaCl. In order to investigate this more closely, we considered PCA plots of the 1.5 %, 6

474   % and 9 % samples separately. It turned out that MgSO$_4$ had strong hydration and

475   denaturation effects already at 6 % concentration, while this was not as pronounced for NaCl

476   (see Fig. 5). At 9 % concentration both salt types gave similar denaturation effects (results not

477   shown), while KCl showed less denaturation even at the 9 % concentration. This finding is in

478   accordance with the Hofmeister series, which attributes SO$_4^{2-}$ with a higher salting-out effect

479   than Cl$^-$ (*47-49*). An increased hydration of the proteins in meat tissue is related to their

480   partial unfolding and to protein destabilization as a final outcome (*44, 50*). This unfolding of

481   the protein can lead to an increase of hydration at moderate salt concentrations, since large

482   parts of the proteins are exposed to the solvent environment and are able to bind water

483   molecules. According to our findings, MgSO$_4$ salt brines increase the hydration properties of

484   myofibrillar proteins more efficiently with increasing salt concentration than NaCl and KCl.

485   Therefore the myofibrillar proteins also denaturate faster with increasing salt concentration in

486   the samples with MgSO$_4$ compared with samples treated with NaCl or KCl. This finding is

487   also supported by measurements of WBC of samples treated with these salts. This may be

488   utilized in meat industry by replacing NaCl partially with lower amounts of MgSO$_4$.

489 As it is shown, FTIR microscopy in combination with chemometrical tools can be used to

490 monitor changes in the muscle proteins caused by different salt types and concentrations. In

491 addition to the most commonly used amide I region, the amide II and water region (3500 –

492 3000 cm^{-1}) are also shown to be sensitive to these minute changes in secondary structure and

493 hydration properties. The water region in particular expressed a potential for assessing the

494 differences in hydration properties in proteins and to supplement the information on

495 secondary structure changes obtained by inspecting amide I region. Moreover, the results

496 obtained by WBC measurements show a high correspondence to the results obtained by FTIR

497 microscopy. This again is showing that the changes in the secondary structure of the

498 myofibrillar proteins can be connected to macroscopic properties of meat, such as WBC.

499 Additionally, although KCl is widely used as a substitute to NaCl (*6, 9, 10*), it showed

500 distinctive differences when it comes to secondary structure of meat proteins and their

501 hydration properties. On the contrary, $MgSO_4$ exhibited certain similarities to NaCl, which

502 might imply that the mechanism of interaction between this salt ions and protein molecules is

503 intrinsically complex.

504

Acknowledgements

511

References

512   **References**

513   1.   Cappuccio, F. P.; Markandu, N. D.; Carney, C.; Sagnella, G. A.; MacGregor, G. A.
514   Double-blind randomised trial of modest salt restriction in older people. *Lancet* **1997,** 350,
515   (9081), 850-854.
516   2.   Cappuccio, F. P.; Kalaitzidis, R.; Duneclift, S.; Eastwood, J. B. Unravelling the links
517   between calcium excretion, salt intake, hypertension, kidney stones and bone metabolism. *J.*
518   *Nephrol.* **2000**, (13), 169-177.
519   3.   Chrysant, G. S. High salt intake and cardiovascular disease: is there a connection?
520   *Nutrition* **2000**, 16, (7-8), 662-664.
521   4.   Ruusunen, M.; Puolanne, E. Reducing sodium intake from meat products. *Meat Sci.*
522   **2005,** 70, (3), 531-541.
523   5.   Desmond, E. Reducing salt: A challenge for the meat industry. *Meat Sci.* **2006,** 74, (1),
524   188-196.
525   6.   Kilcast, D.; Angus, F. *Reducing salt in foods - Practical strategies*. Woodhead
526   Publishing Limited, Cambridge, England: 2007.
527   7.   Offer, G.; Knight, P.; Jeacocke, R.; Almond, R.; Cousins, T.; Elsey, J.; Parsons, N.;
528   Sharp, A.; Starr, R.; Purslow, P. The structural basis of the water-holding, appearance and
529   toughness of meat and meat products. *Food microstruct.* **1989,** 8. , (1), 151-170.
530   8.   He, F. J.; MacGregor, G. A. A comprehensive review on salt and health and current
531   experience of worldwide salt reduction programmes. *J. Hum. Hypertens.* **2008,** 23, (6), 363-
532   384.
533   9.   Guàrdia, M. D.; Guerrero, L.; Gelabert, J.; Gou, P.; Arnau, J. Sensory characterisation
534   and consumer acceptability of small calibre fermented sausages with 50% substitution of
535   NaCl by mixtures of KCl and potassium lactate. *Meat Sci.* **2008,** 80, (4), 1225-1230.
536   10.   Gimeno, O.; Astiasarán, I.; Bello, J. Influence of partial replacement of NaCl with KCl
537   and CaCl2on microbiological evolution of dry fermented sausages. *Food Microbiol.* **2001,** 18,
538   (3), 329-334.
539   11.   Samapundo, S.; Ampofo-Asiama, J.; Anthierens, T.; Xhaferi, R.; Van Bree, I.;
540   Szczepaniak, S.; Goemaere, O.; Steen, L.; Dhooge, M.; Paelinck, H.; Dewettinck, K.;
541   Devlieghere, F. Influence of NaCl reduction and replacement on the growth of Lactobacillus
542   sakei in broth, cooked ham and white sauce. *Int. J. Food Microbiol.* **2010**, 143, (1-2), 9-16.
543   12.   Gou, P.; Guerrero, L.; Gelabert, J.; Arnau, J. Potassium chloride, potassium lactate and
544   glycine as sodium chloride substitutes in fermented sausages and in dry-cured pork loin. *Meat*
545   *Sci.* **1996,** 42, (1), 37-48.
546   13.   Guàrdia, M. D.; Guerrero, L.; Gelabert, J.; Gou, P.; Arnau, J. Consumer attitude
547   towards sodium reduction in meat products and acceptability of fermented sausages with
548   reduced sodium content. *Meat Sci.* **2006,** 73, (3), 484-490.
549   14.   Crehan, C. M.; Troy, D. J.; Buckley, D. J. Effects of salt level and high hydrostatic
550   pressure processing on frankfurters formulated with 1.5 and 2.5% salt. *Meat Sci.* **2000,** 55,
551   (1), 123-130.
552   15.   Selgas, M. D.; Salazar, P.; García, M. L. Usefulness of calcium lactate, citrate and
553   gluconate for calcium enrichment of dry fermented sausages. *Meat Sci.* **2009,** 82, (4), 478-
554   480.
555   16.   Böcker, U.; Ofstad, R.; Bertram, H. C.; Egelandsdal, B. R.; Kohler, A. Salt-Induced
556   Changes in Pork Myofibrillar Tissue Investigated by FT-IR Microspectroscopy and Light
557   Microscopy. *J. Agric. Food Chem.* **2006,** 54, (18), 6733-6740.
558   17.   Wu, Z.; Bertram, H. C.; Boecker, U.; Ofstad, R.; Kohler, A. Myowater Dynamics and
559   Protein Secondary Structural Changes As Affected by Heating Rate in Three Pork Qualities:

A Combined FT-IR Microspectroscopic and 1H NMR Relaxometry Study. *J. Agric. Food Chem.* **2007,** 55, (10), 3990-3997.

18.　　Bertram, H. C.; Kohler, A.; Bocker, U.; Ofstad, R.; Andersen, H. J. Heat-induced changes in myofibrillar protein structures and myowater of two pork qualities. A combined FT-IR spectroscopy and low-field NMR relaxometry study. *J. Agric. Food Chem.* **2006,** 54, (5), 1740-1746.

19.　　Maréchal, Y. Interaction configurations of H2O molecules in a protein (Stratum Corneum) by infrared spectrometry. *J. Mol. Struct.* **1997,** 416, (1-3), 133-143.

20.　　Jackson, M.; Mantsch, H. H. The Use and Misuse of FTIR Spectroscopy in the Determination of Protein Structure. *Crit. Rev. Biochem. Mol. Biol.* **1995,** 30, (2), 95-120.

21.　　Grdadolnik, J. A FTIR investigation of protein conformation. *Bull. Chem. Technol. Maced* **2002,** 21, 23–34.

22.　　Barth, A. Infrared spectroscopy of proteins. *Biochim. Biophys. Acta (BBA) - Bioenerg.* **2007,** 1767, (9), 1073-1101.

23.　　Wierbicki, E.; Deatherage, F. E. Water Content of Meats, Determination of Water-Holding Capacity of Fresh Meats. *J. Agric. Food Chem.* **1958,** 6, (5), 387-392.

24.　　Savitzky, A.; Golay, M. Smoothing and differentiation of data by simplified least squares procedures. *Anal. Chem.* **1964,** 36, (8), 1627-1639.

25.　　Kohler, A.; Kirschner, C.; Oust, A.; Martens, H. Extended multiplicative signal correction as a tool for separation and characterization of physical and chemical information in Fourier transform infrared microscopy images of cryo-sections of beef loin. *Appl. Spectrosc.* **2005,** 59, (6), 707-716.

26.　　Martens, H.; Nielsen, J. P.; Engelsen, S. B. Light scattering and light absorbance separated by extended multiplicative signal correction. Application to near-infrared transmission analysis of powder mixtures. *Anal. Chem.* **2003,** 75, (3), 394-404.

27.　　Martens, H.; Næs, T. *Multivariate Calibration*. John Wiley & Sons: Chichester, 1989.

28.　　Martens, H.; Martens, M. Multivariate Analysis of Quality. An Introduction. *Meas. Sci. Technol.* **2001,** 12, (10), 1746.

29.　　Golub, G. H.; Heath, M.; Wahba, G. Generalized Cross-Validation as a Method for Choosing a Good Ridge Parameter. *Technometrics* **1979,** 21, (2), 215-223.

30.　　Efron, B. Estimating the Error Rate of a Prediction Rule: Improvement on Cross-Validation. *J. Am. Stat. Assoc.* **1983,** 78, (382), 316-331.

31.　　Bocker, U.; Ofstad, R.; Wu, Z. Y.; Bertram, H. C.; Sockalingum, G. D.; Manfait, M.; Egelandsdal, B.; Kohler, A. Revealing covariance structures in Fourier transform infrared and Raman microspectroscopy spectra: A study on pork muscle fiber tissue subjected to different processing parameters. *Appl. Spectrosc.* **2007,** 61, (10), 1032-1039.

32.　　Barth, A.; Zscherp, C. What vibrations tell about proteins. *Q. Rev Biophys.* **2002,** 35, (04), 369-430.

33.　　Böcker, U.; Ofstad, R.; Wu, Z.; Bertram, H. C.; Sockalingum, G. D.; Manfait, M.; Egelandsdal, B.; Kohler, A. Revealing Covariance Structures in Fourier Transform Infrared and Raman Microspectroscopy Spectra: A Study on Pork Muscle Fiber Tissue Subjected to Different Processing Parameters. *Appl. Spectrosc.* **2007,** 61, (10), 1032-1039.

34.　　Surewicz, W. K.; Mantsch, H. H.; Chapman, D. Determination of protein secondary structure by Fourier transform infrared spectroscopy: A critical assessment. *Biochemistry* **1993,** 32, (2), 389-394.

35.　　Manas, E.; Getahun, Z.; Wright, W.; DeGrado, W.; Vanderkooi, J. Infrared spectra of amide groups in -helical proteins: Evidence for hydrogen bonding between helices and water. *J. Am. Chem. Soc* **2000,** 122, (41), 9883-9890.

36. Boubellouta, T.; Galtier, V.; Dufour, É. Structural Changes of Milk Components During Acid-Induced Coagulation Kinetics as Studied by Synchronous Fluorescence and Mid-Infrared Spectroscopy. *Appl. Spectrosc.* **2010**, 65, (3), 284-292.

37. Nevskaya, N. A.; Chirgadze, Y. N. Infrared spectra and resonance interactions of amide-I and II vibrations of α-helix. *Biopolymers* **1976,** 15, (4), 637-648.

38. Rothschild, K. J.; Clark, N. A. Polarized infrared spectroscopy of oriented purple membrane. *Biophys. J.* **1979,** 25, (3), 473-487.

39. Liltorp, K.; Maréchal, Y. Hydration of lysozyme as observed by infrared spectrometry. *Biopolymers* **2005,** 79, (4), 185-196.

40. Barth, A. The infrared absorption of amino acid side chains. *Progr. Biophys. Mol. Biol.* **2000,** 74, (3-5), 141-173.

41. Fabian, H.; Schultz, C. P. *Fourier Transform Infrared Spectroscopy in Peptide and Protein Analysis*. John Wiley & Sons, Ltd: 2006.

42. Abe, Y.; Krimm, S. Normal vibrations of crystalline polyglycine I. *Biopolymers* **1972,** 11, (9), 1817-1839.

43. Bertram, H. C.; Kohler, A.; Boecker, U.; Ofstad, R.; Andersen, H. J. Heat-Induced Changes in Myofibrillar Protein Structures and Myowater of Two Pork Qualities. A Combined FT-IR Spectroscopy and Low-Field NMR Relaxometry Study. *J. Agric. Food Chem.* **2006,** 54, (5), 1740-1746.

44. Stigter D.; Aalonso D. O. V.; Dill K. A. *Protein stability : electrostatics and compact denatured states*. National Academy of Sciences: Washington, DC, ETATS-UNIS, 1991; Vol. 88, p 5.

45. Dill, K. A. Dominant forces in protein folding. *Biochemistry* **1990,** 29, (31), 7133-7155.

46. Ishii, Y. The local and global unfolding of coiled-coil tropomyosin. *Eur. J. Biochem.* **1994,** 221, (2), 705-712.

47. Baldwin, R. L., How Hofmeister ion interactions affect protein stability. *Biophys. J.* **1996,** 71, (4), 2056-2063.

48. Giner, I.; Pera, G.; Lafuente, C.; López, M. C.; Cea, P. Influence of the Hofmeister series of anions on the molecular organization of positively ionized monolayers of a viologen derivative. *J. Colloid Interface Sci.* **2007,** 315, (2), 588-596.

49. Lawal, O. S. Kosmotropes and chaotropes as they affect functionality of a protein isolate. *Food Chem.* **2006,** 95, (1), 101-107.

50. Hofmeister, F. Zur lehre von der wirkung der salze. *Naunyn-Schmiedeberg's Arch. Pharmacol.* **1888,** 25, (1), 1-30.

51. Wu, Z.; Bertram, H. C.; Kohler, A.; Boecker, U.; Ofstad, R.; Andersen, H. J. Influence of Aging and Salting on Protein Secondary Structures and Water Distribution in Uncooked and Cooked Pork. A Combined FT-IR Microspectroscopy and 1H NMR Relaxometry Study. *J. Agric. Food Chem.* **2006,** 54, (22), 8589-8597.

52. Pevsner, A.; Diem, M. Infrared Spectroscopic Studies of Major Cellular Components. Part I: The Effect of Hydration on the Spectra of Proteins. *Appl. Spectrosc.* **2001,** 55, (6), 788-793.

53. Silvestrelli, P. L.; Bernasconi, M.; Parrinello, M., Ab initio infrared spectrum of liquid water. *Chem. Phys. Lett.* **1997,** 277, (5-6), 478-482.

54. Taylor, J. R. *An introduction to error analysis: the study of uncertainties in physical measurements*. University Science Books: 1997.

657 **Tables**

658 **Table 1:** Band positions and assignments for the amide I, amide II and water region according

659 to literature and our previous work

Region	Freq. (cm⁻¹)	Tentative assignment
amide I 1700-1600 cm⁻¹ (80 % C=O stretch, 10 % C-N stretch, 10 % N-H bend)	1693	Aggregated β-sheet structures (side band of 1631 cm⁻¹ band) (*32-35*), M/P
	1682	Native (parallel/antiparallel) β-sheet structures (*20, 32, 33, 37*), M/P/T
	1674	Tentatively assigned to turns (*22*), M/P
	1667	Non-hydrogenated C=O group, internal random coil segments that are not involved in H-bonding (*33, 35*), M/P
	1660	Loop structures / α-helical structures (*16, 43, 51*), M/P
	1655	α-helical structures, C=O stretching vibrations originating from α-helical structures in the myofibrillar proteins (*20, 32, 33, 37*), M/P/T or water vibration (*36, 38*) P
	1638	water deformation mode in liquid water (*19, 52*) P or native (parallel/antiparallel) β-sheet structures (*22, 33*), M/P/T
	1631	Aggregated β-sheet structures (*32-35*), M/P
	1618	Aggregated β-sheet structures (*16, 43, 51*), M
	1611	Tyrosine amino-acid side chain vibrations (*33, 40*), or aggregated strands (*41*), M/P
amide II 1600-1500 cm⁻¹ (60 % N–H bend, 40 %C–N stretch)	1594	Not assigned
	1584	α-helical structures (*33*), M
	1575	Amide II unspecified (*33*), M
	1567	Residue and/ or possibly aggregated β-sheet structures (*33, 42*), M
	1547	α-helical structures (*33*), M/ P
	1537	Possibly aggregated β-sheet structures (*33*), M
	1516	Possibly tyrosine (*33*), M/P
water region	3473	Non-hydrogenated N-H groups (*19, 22, 39*), P

3500-3000 cm^{-1} (N-H stretching C-N-H stretching vibration O-H stretching vibration)	3420	Hydrogenated N-H groups or O-H stretching band (*21, 22, 39, 53*), T/P
	3361	Companion band of 1530 cm^{-1} band, in solution occurring at 3345 cm^{-1} and/or N-H stretching band (*21, 39*), T/P
	3290	N-H stretching band / amide A (*21, 22, 39, 42*), T/P or hydrogen bonded NH groups (*19*) P
	3190	Not assigned
	3063	N-H stretch / amide B / amide II overtone / amide II combination mode in −sheet structures (*22, 39*), T/P
	3035	Not assigned

660 * **M** = obtained in real meat system; **P** = obtained in pure protein or polypeptide model system; **T** = obtained by

661 theoretical calculation and/or prediction

662

663

Figure Captions

666   **Figure 1**: (a) A typical FTIR spectrum presented in the whole spectral region from 4000-1000

667   cm^{-1}. Second derivatives of each of the selected regions are shown for the water region (b),

668   the amide I (c) and the amide II region (d).

669

670   **Figure 2:** PCA score plots for first and second PCs are shown for the amide I region (a and b)

671   and the water region (c and d). In the first column, (a) and (c), samples are labeled according

672   to the salt concentration, while in the second column, (b) and (d), samples are labeled

673   according to the salt type.

674

675   **Figure 3:** Correlation loading plots of the first and second components for PCA models of the

676   amide I region and the water region are shown in (a) and (b) respectively. Pacified design

677   variables are plotted in green color including interactions between different salt

678   concentrations and different salt types.

679

680   **Figure 4:** Correlation loading plots of the first and second component for PLSR models using

681   the water region as *X* and amide I region as *Y* are shown in (a), while (b) shows the

682   corresponding correlation loading plot using the amide II region as *Y*. Water region variables

683   are plotted in black color, amide I in blue, while pacified design variables are designated with

684   green color.

685

686   **Figure 5:** Correlation loading plot of the first and second component for PLSR model using

687   the water region as *X* and amide I region as *Y*. This PLSR model is calculated for 6 %

688   concentrations only. Water region variables are plotted in black color, amide I in blue, while

689   pacified amide II and design variables are depicted with red and green color respectively.

690

691   **Figure 6:** Water Binding Capacity of samples treated with different salt brines plotted with

692   twofold standard deviation of the mean value (corresponding to a 95 % confidence interval)

693   (*54*): light gray bars represent the 1.5 % concentration, middle gray bars 6 % and dark gray

694   bars 9 % concentration, while first three bars depict NaCl brines, second three MgSO$_4$ brines

695   and last three KCl brines.

696

697   **Figures**

698   Figure 1

699

a

b

c
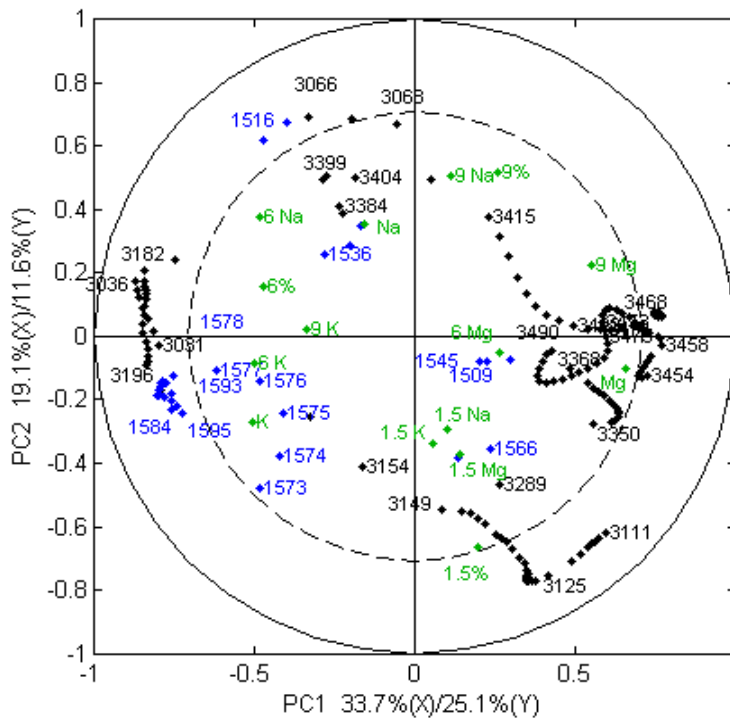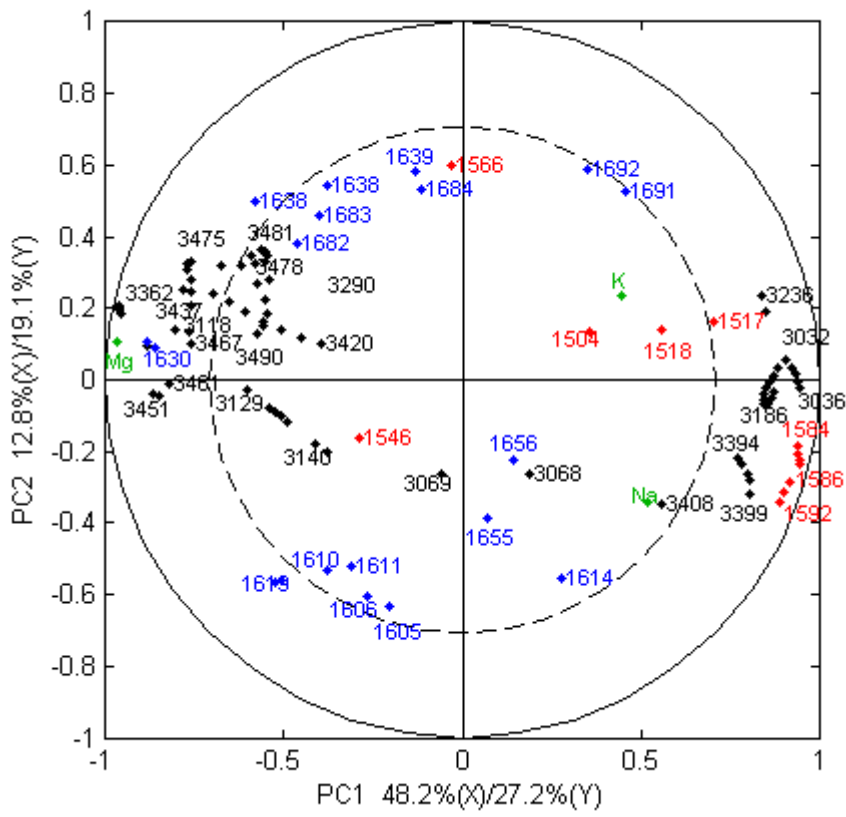
d
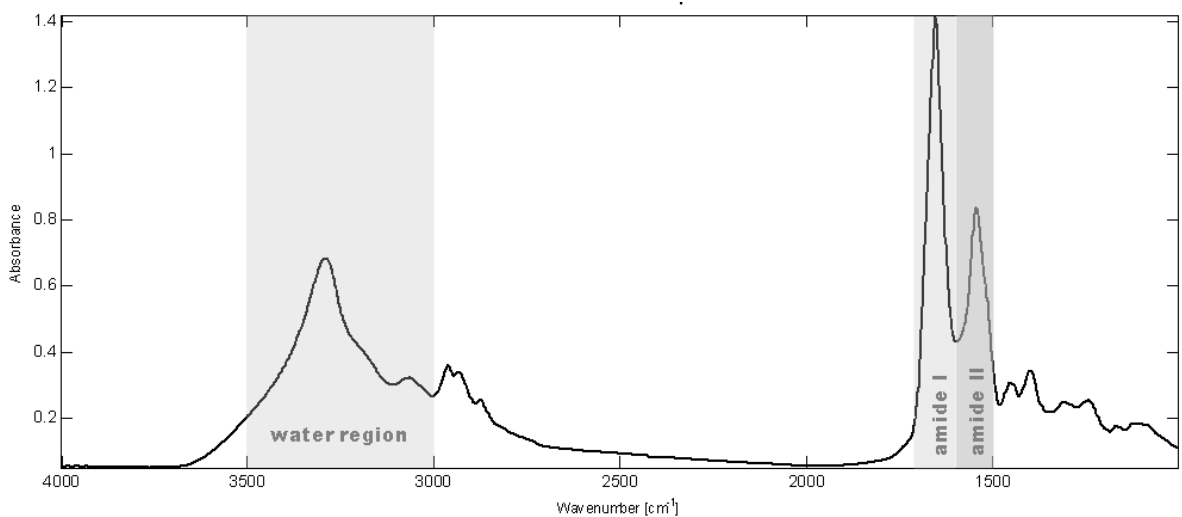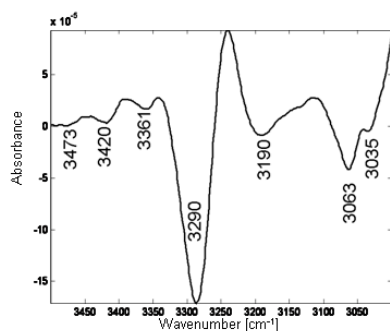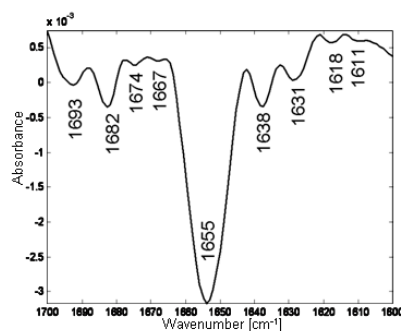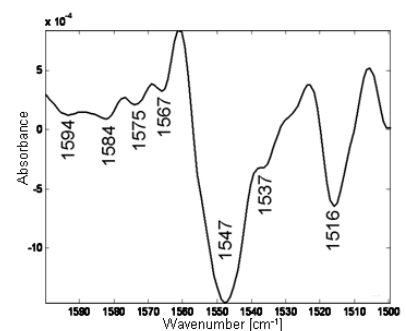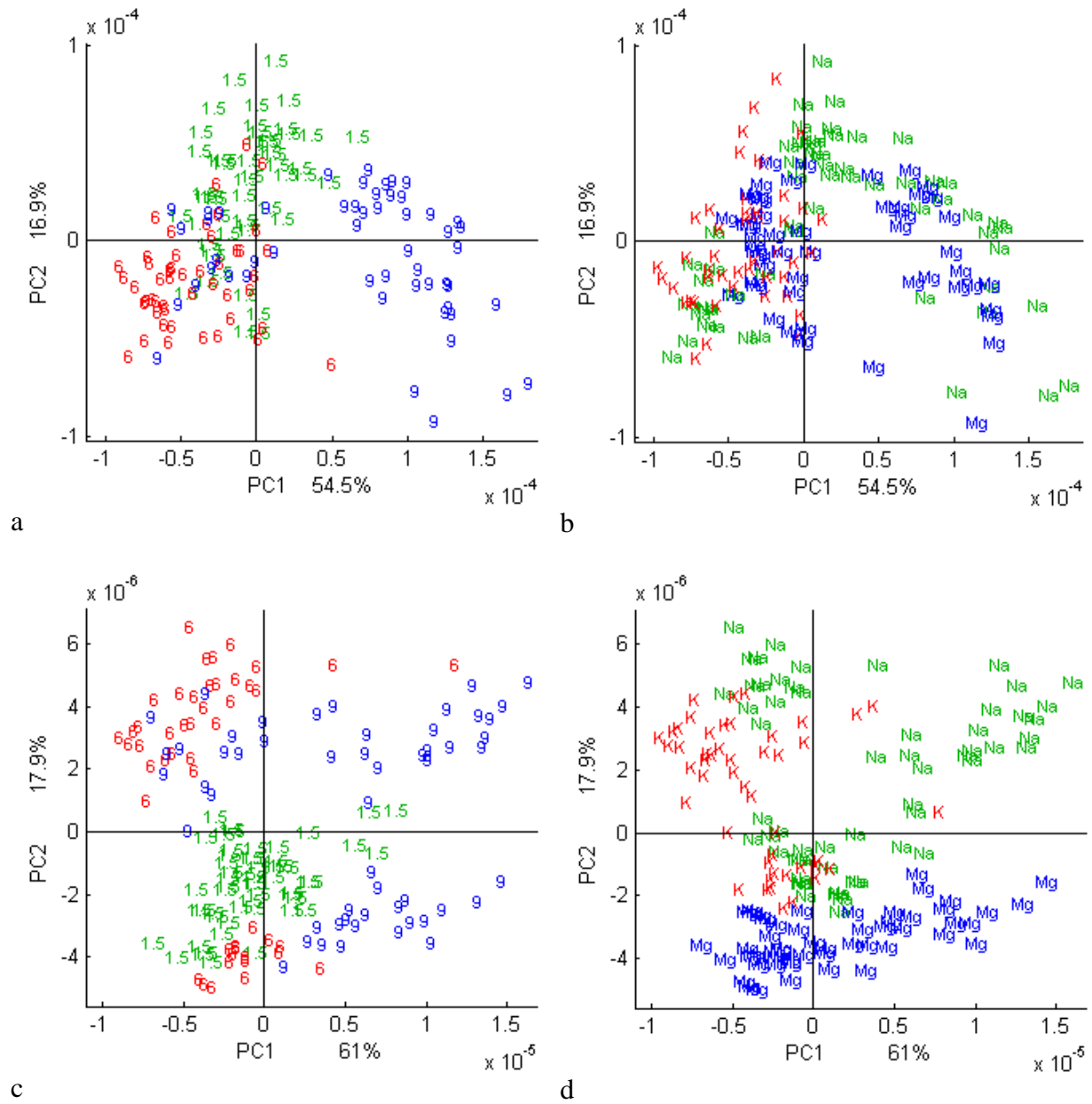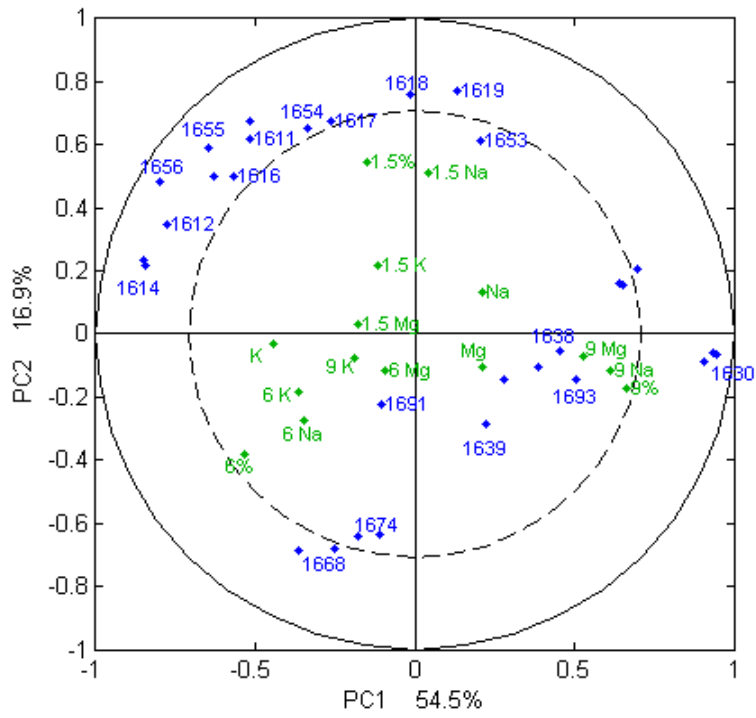
Figure 2

a
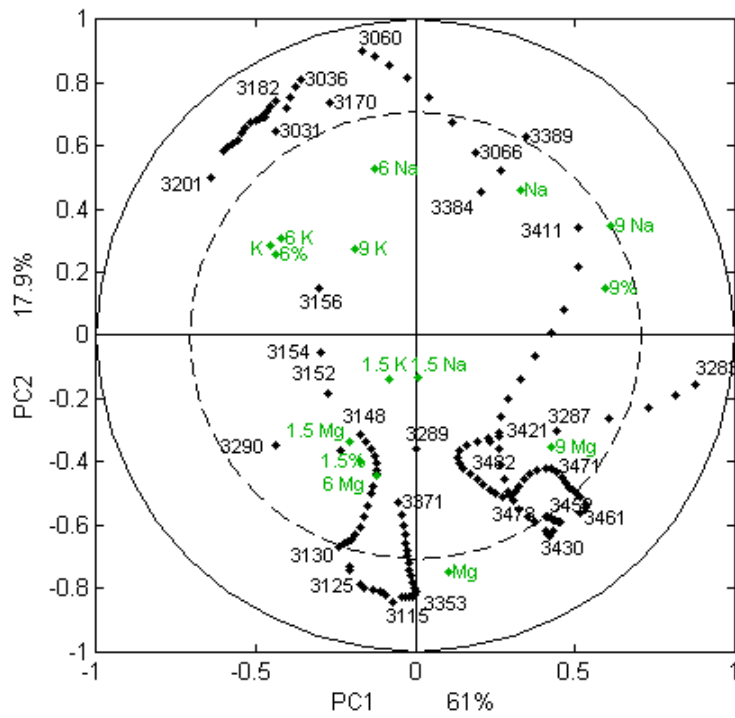
b

702   Figure 3

703
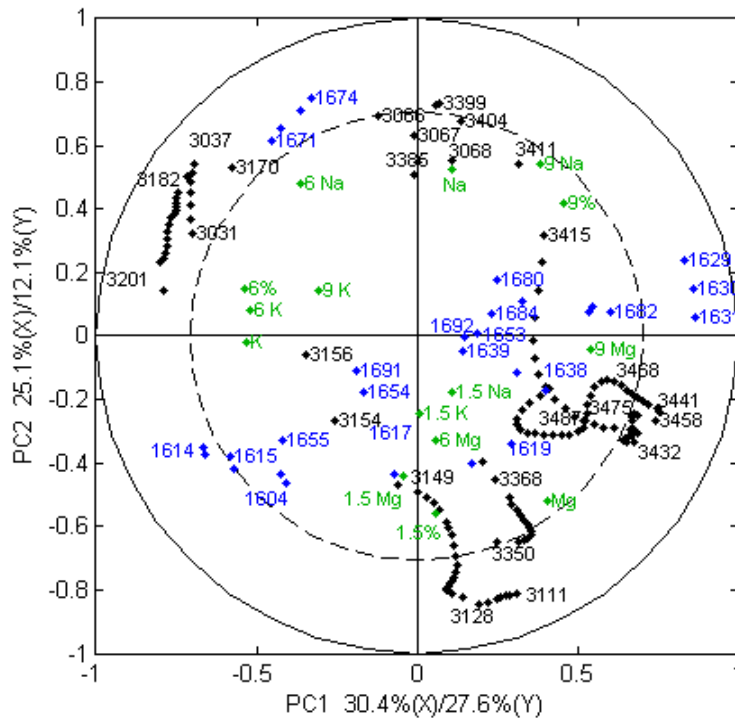
a

b

704   Figure 4

705

706   Figure 5

707

727   Figure 6

728

729